Since January 2020 Elsevier has created a COVID-19 resource centre with free information in English and Mandarin on the novel coronavirus COVID-19. The COVID-19 resource centre is hosted on Elsevier Connect, the company's public news and information website.

Separation and Purification Technology 282 (2022) 120049

Contents lists available at ScienceDirect

Separation and Purification Technology

journal homepage: www.elsevier.com/locate/seppur

Filtering efficiency model that includes the statistical randomness of non-woven fiber layers in facemasks

B.T.H. Borgelink [a,1,*], A.E. Carchia [a,b,1], J.F. Hernández-Sánchez [c], D. Caputo [b], J.G. E. Gardeniers [a,*], A. Susarrey-Arce [a,*]

[a] Mesoscale Chemical Systems, MESA+ Institute, University of Twente, Drienerlolaan 5, 7522 NB Enschede, the Netherlands
[b] Department Information Engineering, Electronics and Telecommunications, Sapienza University of Rome, via Eudossiana 18, 00184 Rome, Italy
[c] Instituto de Ciencias Aplicadas y Tecnología, Universidad Nacional Autónoma de México, Circuito Exterior S/N, Ciudad universitaria, 04510, Mexico City

ARTICLE INFO

Keywords:
COVID-19
Facemasks
Nanodroplets
Filtration efficiency
CFD modeling

ABSTRACT

Facemasks have become important tools to fight virus spread during the recent COVID-19 pandemic, but their effectiveness is still under debate. We present a computational model to predict the filtering efficiency of an N95-facemask, consisting of three non-woven fiber layers with different particle capturing mechanisms. Parameters such as fiber layer thickness, diameter distribution, and packing density are used to construct two-dimensional cross-sectional geometries. An essential and novel element is that the polydisperse fibers are positioned randomly within a simulation domain, and that the simulation is repeated with different random configurations. This strategy is thought to give a more realistic view of practical facemasks compared to existing analytical models that mostly assume homogeneous fiber beds of monodisperse fibers. The incompressible Navier-Stokes and continuity equations are used to solve the velocity field for various droplet-laden air inflow velocities. Droplet diameters are ranging from 10 nm to 1.0 μm, which covers the size range from the SARS-CoV-2 virus to the large virus-laden airborne droplets. Air inflow velocities varying between 0.1 $m{\cdot}s^{-1}$ to 10 $m{\cdot}s^{-1}$ are considered, which are typically encountered during expiratory events like breathing, talking, and coughing. The presented model elucidates the different capturing efficiencies (i.e., mechanical and electrostatic filtering) of droplets as a function of their diameter and air inflow velocity. Simulation results are compared to analytical models and particularly compare well with experimental results from literature. Our numerical approach will be helpful in finding new directions for anti-viral facemask optimization.

1. Introduction

In late December 2019, an outbreak of a coronavirus strain (SARS-CoV-2) was reported in Wuhan, China. At the time when this manuscript was written, the virus has spread worldwide, and the COVID-19 infected over 190 million people, causing more than 4 million deaths [1]. COVID-19 is a highly transmissible respiratory disease, and the primary transmission route is through mucosae contact with respiratory droplets generated when an infected person coughs, sneezes, talks [2], or breaths. Virus-laden droplets or aerosols having a diameter below 5 μm are claimed to be relevant for transmission even beyond the recommended social distance because they remain suspended in the air in indoor environments for hours, during which they may infect individuals [3,4]. A schematic representation of the main transmission route is depicted in Fig. 1, in which the airborne droplets laden with SARS-CoV-2 are color-coded to size. An infected individual generates airborne droplets on the left, which are inhaled by the person on the right.

One of the measures to reduce the SARS-CoV-2 virus spreading rate recommended by health organizations and governments is the use of a facemask [5,6]. The widespread usage of this protective equipment has been crucial for epidemic containment both in the first and second waves of COVID-19 [7–9]. However, controversies addressing people's adherence to facemask usage still exist because of the breathing discomfort and the unclear protection offered.

An open issue is the filtering efficiency of facemasks against nano-

* Corresponding authors at: Arturo Susarrey-Arce: Mesoscale Chemical Systems, MESA+ Institute for Nanotechnology, University of Twente, PO. Box 217, Enschede 7500AE, The Netherlands.
E-mail addresses: b.t.h.borgelink@utwente.nl (B.T.H. Borgelink), j.g.e.gardeniers@utwente.nl (J.G.E. Gardeniers), a.susarreyarce@utwente.nl (A. Susarrey-Arce).
[1] These authors contributed equally to this work.

https://doi.org/10.1016/j.seppur.2021.120049
Received 31 July 2021; Received in revised form 18 October 2021; Accepted 28 October 2021
Available online 1 November 2021

metric droplets (small-sized droplets in Fig. 1).[10] Recent studies pointed out that viruses, such as SARS-CoV-2, can be transmitted via airborne droplets with a diameter ranging from 60 to 300 nm [11]. Existing protective filtration equipment is customarily not tested for airborne particles smaller than 300 nm. For example, according to the National Institute for Occupational Safety and Health (NIOSH), N95-grade facemasks must ensure a 95% capturing efficiency of 300nm-diameter particles, while the pressure drop across the face mask should be less than 250 Pa, at an air inflow rate of 85 L min^{-1} [12]. A new standardized test protocol might be required to adequately study the filtering efficiency of smaller droplets and reduce the spread of the SARS-CoV-2 virus [10,13].

An N95-facemask (Fig. 2**a-b**) consists of three layers with different layer properties, such as layer thickness and morphology. The outer fibrous layers, 1 and 3 in Fig. 2**a-b**, stabilize and protect the inner layer. The inner layer, layer 2 in Fig. 2**a-b**, consists of thin electret fibers generating an inhomogeneous electric field between the fibers. This layer function is two-fold: (i) it acts as a mechanical filter, and (ii) it deflects droplets through electrostatic interaction and thereby increasing the filtration efficiency [14–16]. The distinct mechanisms to capture airborne droplets and fine solid particles suspended in air (aerosols) are inertial impaction, interception, Brownian diffusion, and electrostatic interaction. Each of them is schematically depicted in Fig. 2**c**.

As a background for our numerical model to analyze the facemask filtering efficiency, we first give a short review of existing models developed by others. To analytically describe the fluid flow through a fiber bed, Kuwabara's model is often used. In this model, the fiber bed is represented by a 2D array of monodisperse cylindrical fibers, positioned randomly but distributed homogeneously. A coaxial periphery around the fibers is defined at which the airflow around neighboring fibers causes the vorticity to disappear. In Kuwabara's model, the packing density α is defined as the ratio between the cross-sectional surface area of the fiber and the surface area of the mentioned coaxial periphery. The flow field between the fiber bed is defined as a function of the packing density. Inside a fiber bed, a fluid traverses a tortuous path, meaning that the air velocity between the fibers is higher than the air flowing into the fiber bed. Kuwabara represented this velocity enhancement as the inverse of the hydrodynamic factor Ku, defined as $Ku = -\frac{1}{2}\ln\alpha - \frac{3}{4} + \alpha - \frac{\alpha^2}{4}$ [17]. Because the hydrodynamic factor is a function of the packing density only, it can also be employed as a measure of the packing density of a fiber bed.

A few dimensionless numbers are introduced to characterize the flow inside the fiber geometry and the droplet capturing mechanisms. Droplets of diameter d_d suspended in a flow are well advected by the fluid flow if their characteristic response time is smaller than that of the fluid. The Stokes number Stk is the ratio between these two characteristic time scales and is calculated as $Stk = \frac{Cu\rho_d d_d^2 V}{18\mu\overline{d_f}}$, with ρ_d, V, μ and $\overline{d_f}$ the droplet density, air inflow velocity, dynamic air viscosity and mean fiber diameter, respectively [18]. Cu is the Cunningham slip factor, defined as $Cu = 1 + \frac{\lambda}{d_d}\left(2.31 + 0.942\exp\left(-0.298\frac{d_d}{\lambda}\right)\right)$, with λ the mean free path of the fluid molecules, which is approximately 67 nm in the air at room temperature and atmospheric pressure [19,20]. The Stokes drag force, which is causing the droplets suspended in the air to move, assumes no-slip of the air molecules at the surface of the droplet. However, if the droplet size is of the order of the mean free path, air cannot be considered a continuum anymore. The slip factor assures that the drag force acting on small droplets can still be calculated [19]. If $Stk \ll 1$, the droplets are well advected by the flow, whereas Stk greater than 1 represents droplets that do not follow the liquid streamlines due to their inertia. The Reynolds number Re is defined as the ratio between inertial and viscous forces occurring in the airflow and is calculated as $Re = \frac{\rho_a V \overline{d_f}}{\mu}$, with ρ_a the density of air moving between the fibers [21]. It is found that for air flowing through an N95-facemask, $Re \leq 20$, meaning that the airflow is laminar. The ratio between droplets moving by means of advection and (Brownian) diffusion is characterized by the Péclet number Pe. For creeping and laminar flows, the Péclet number is defined as $Pe = \frac{3\pi\mu V d_d \overline{d_f}}{k_b T}$, with k_b the Boltzmann constant and T the air temperature. Droplets that are moving in a diffusive regime are characterized by $Pe < 1$ [22]. The Péclet number does not contain the Cunningham slip factor, because the models presented later correct for the slip effect differently. For the ease of writing, the ratio between the droplet diameter and fiber diameter is defined as R, i.e., $R = \frac{d_d}{\overline{d_f}}$.

The capturing efficiency of a single fiber is defined as the probability that a droplet moving along a single fiber is captured by making contact with the fiber. If droplet-laden air moves along the fiber surface, the droplet path may deviate from the air streamlines due to its inertia. Inertial impaction relies on such deviations, where droplets impact the fibers due to their inertia (Fig. 2**c**).[16,15,18] Zhu et al. found that the single fiber capturing efficiency by means of inertial impaction is

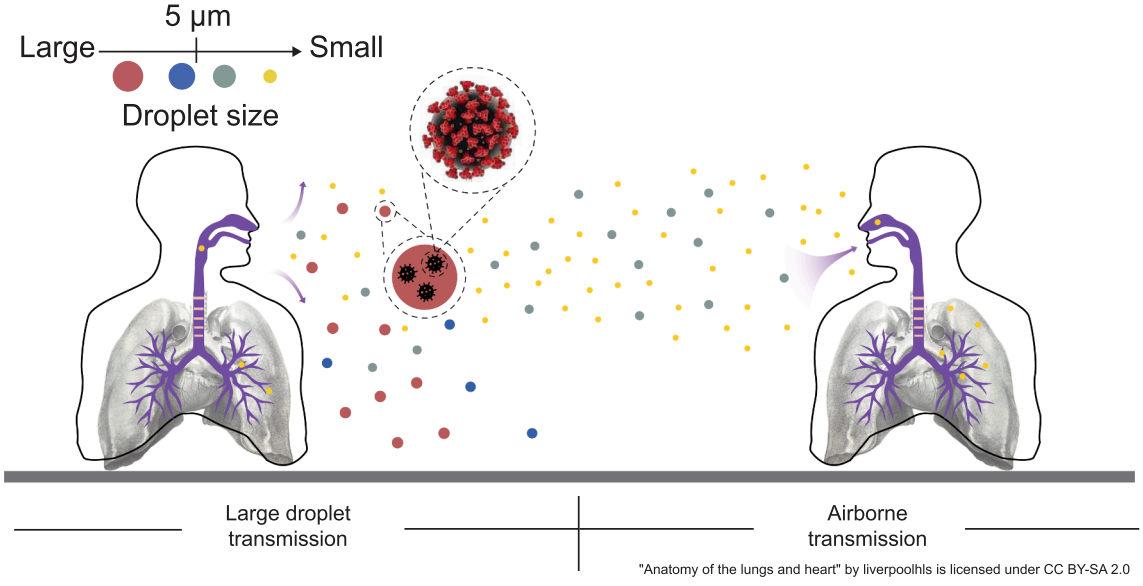

Fig. 1. Schematic representation of the main transmission routes of the SARS-CoV-2 virus.

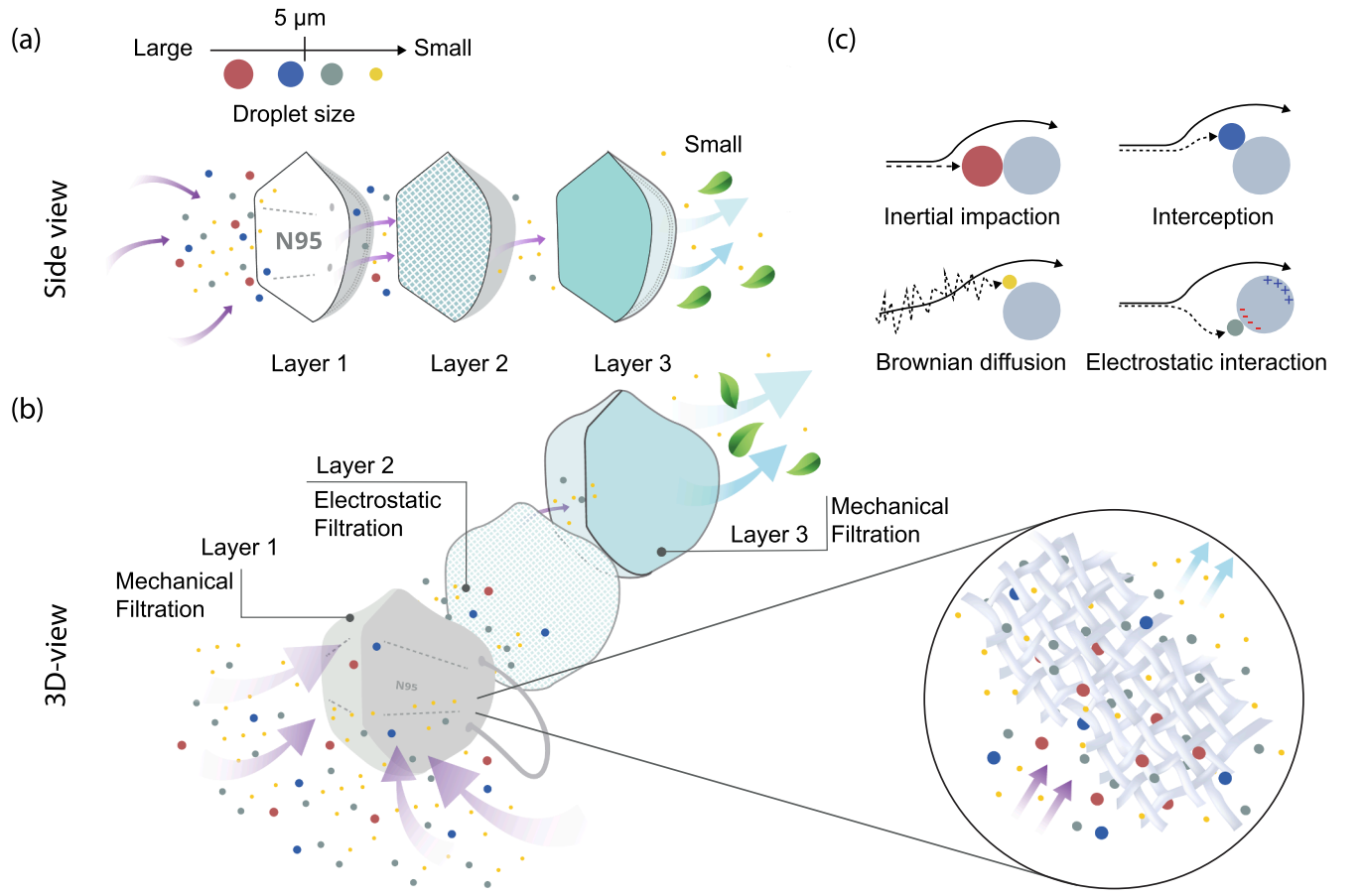

Fig. 2. (a) 2D and (b) 3D schematic drawing of an N95-facemask composed of three layers. (c) 2D-schematic representation of the different capturing mechanisms considered in this study.

calculated as $E_I = \frac{2(1-\alpha)\sqrt{\alpha}R}{Ku} Stk + \frac{(1-\alpha)\alpha}{Ku} Stk^2$ [18].

Interception is a mechanism in which the droplet moves along the streamline surrounding the fiber but still is captured due to its size (Fig. 2**c**).[15,16,20,23–25] The droplets moving in the air are constantly colliding with surrounding air molecules. As a result, small droplets move in random paths due to Brownian diffusion and, thereby, could hit the fiber surface (Fig. 2**c**).[15,16,20,23,24] Lee and Liu theoretically predicted the capturing efficiency by means of both interception and Brownian diffusion using the Kuwabara flow field and corrected their models to fit available experimental data [20]. Subsequently, Liu and Rubow [25] and Payet et al. [24] made refinements to this model to account for slip effects on droplets of sizes comparable to the mean free path of air molecules λ, and to restrict the single fiber capturing mechanism to not exceed $E_D = 1$. The single fiber capturing efficiency by means of interception E_R and diffusion E_D are calculated as $E_R = 0.6 \frac{1-\alpha}{Ku} \frac{R^2}{1+R} C_R$ and $E_D = \frac{1.6\left(\frac{1-\alpha}{Ku}\right)^{\frac{1}{3}} Pe^{-\frac{2}{3}} C_D}{1+1.6\left(\frac{1-\alpha}{Ku}\right)^{\frac{1}{3}} Pe^{-\frac{2}{3}} C_D}$, respectively. [24,25]. In these equations, the constants 0.6 and 1.6 are introduced to fit the model with experimental data, and C_R and C_D are correction factors to account for the slip effect and are calculated as $C_R = 1 + \frac{3.998\lambda}{d_d}$ and $C_D = 1 + 0.776 \frac{\lambda}{d_f} \left(\frac{(1-\alpha)Pe}{Ku}\right)^{1/3}$ [24,25]. Because the density of streamlines around the fiber is independent of the air velocity, the single fiber capturing efficiency by means of interception is also found to be independent of the flow velocity. Due to Brownian motion of the droplets, they may change to another streamline closer to the fiber surface. It has experimentally been shown that the single fiber capturing efficiencies by means of diffusion and interception enhance each other. Hence, they are combined as $E_{DR} = E_D + E_R$.

An electret can be seen as the electric equivalent of a magnet. Its surface contains either positive or negative bound electric charge. As a consequence, an electret generates an external electric field. Droplets moving through an electret fiber bed are exposed to this electric field, which polarizes them and causes a dielectrophoretic force to act on them. This force deflects the droplets and drives them towards regions of a high diverging electric field, thereby capturing them (Fig. 2**c**) [24–28]. Bałazy et al. [28] adapted the model from Lathrache and Fissan [29–31] to fit the single fiber collection efficiency by means of dielectrophoresis, calculated as $E_E = 0.21 \left(\frac{1-\alpha}{Ku}\right)^{\frac{2}{5}} \frac{\pi C_E}{1+2\,\pi C_E^{\frac{2}{3}}}$, with C_E the electrostatic capturing parameter defined as $C_E = \frac{Cuq^2 d_d^2}{3\pi\epsilon_0 \mu d_f^3 \left(1+\epsilon_{r,f}\right)^2} V \left(\frac{\epsilon_{r,d}-1}{\epsilon_{r,d}+2}\right)$. In these equations, ϵ_0 is the vacuum permittivity, $\epsilon_{r,f}$ the dielectric constant of the fiber material, $\epsilon_{r,d}$ the dielectric constant of the liquid in the droplets and q the line charge density of the electret fibers. The electric field strength around an electret fiber is proportional to the permanent dipole moment, thus proportional to the bound charge density at the surface of the fiber. The line charge density is not a physically meaningful quantity to measure the dipole strength of the electret fibers and often is treated as a fitting parameter. Reported line charge density values vary between $q = 0.06$ nC m^{-1} to $q = 34.2$ nC m^{-1} [28]. This large spread of three orders of magnitude is assumed to be caused by different data fitting protocols and differences in the electret fibers' permanent dipole moment.

Facemask filters are made of non-woven fiber webs and are classified

as depth-filters. Thus, when droplets smaller than the average distance between fibers are passing through the web, different mechanisms intervene simultaneously to capture them. Customarily, the depth-filtration theory is employed to calculate the overall droplet capturing efficiency E of a fiber bed from the single fiber capturing efficiency E_f.[15,16] This theory assumes that air is flowing perpendicularly to the fiber surface and not along with the fiber. The single fiber capturing mechanisms E_I, E_{DR} and E_E discussed in the introduction are assumed to act independently on the droplet, i.e. these capturing mechanisms do not enhance or reduce the efficiency due to another capturing mechanism. Based on this assumption, the single fiber capturing efficiency E_f is calculated as $E_f = 1 - \prod_j (1 - E_j)$, with E_j the corresponding relative is capturing efficiency of each capturing mechanism, which are E_I, E_{DR} and E_E.[15,16] The overall capturing efficiency E of a fiber bed consisting of parallel fibers is calculated as $E = 1 - \exp\left(\frac{-4\alpha E_f L}{\pi \overline{d_f}(1-\alpha)}\right)$.[15,16,32] Although the formal derivation can be found in Davies, [32] an intuitive understanding of this equation is given here. Consider a droplet concentration difference between the front and back sides of the facemask. The chance that a droplet collides onto a single fiber rather than passes it is proportional to the cross-sectional area of the fiber. In terms of the packing density, this surface is proportional to $\frac{4\alpha}{\pi \overline{d_f}}$. The larger the thickness L of the fiber bed, the higher the probability a droplet gets captured by the fiber. The increase of the air velocity inside the fiber bed, because of the tortuous path it has to take, scales inversely with $1-\alpha$. This factor is taken into account, as a higher flow velocity inside the fiber bed results in a larger droplet flux towards a single fiber. Hence, the exponent scales as $\frac{L}{1-\alpha}$, too.

Lee and Liu realized that different capturing mechanisms do not act independently and combined the single fiber capturing mechanisms through diffusion and interception [20]. In reality, different capturing mechanisms will act cooperatively and enhance the capturing efficiency. Most of the reported models are only reasonably accurate for a specific set of conditions such as droplet diameter, flow velocity, or dielectric constant of the droplets. Furthermore, in a real fiber bed with randomly distributed polydisperse fibers, fibers can be located close to each other or touch and cross each other. Thus, the calculation of the capturing efficiency by means of the depth filtration theory is not only an elaborative task, its accuracy can be unsatisfactory.

In the design and optimization process of multi-layered filters, computer modeling is a very powerful tool [33]. A model that predicts the capturing efficiency of a fiber bed for different-sized droplets as a function of the air inflow velocity reduces the necessity of performing tedious and expensive measurements to determine the facemask performance. The electric field and airflow field simulation between the fibers and the droplet trajectories through the fibrous layers offer an excellent method to study mechanical and electrostatic filtration mechanisms. This allows a quantitative and qualitative understanding of the filtration process, and in our view, is more intuitive than existing analytical models. Furthermore, and in our view very relevant for practical implementation, a numerical model allows straightforward randomization of the fiber diameter and location of the fibers, thereby producing statistical data with increased reliability, because it takes into account the variability in real facemasks, which occurs due to the mask-to-mask variation in the production process, and due to the variation in mask position and configuration during wearing.

In our work, a 2D computational model has been developed using COMSOL Multiphysics® to predict the filtering efficiency of each layer of an N95-facemask (Fig. 2**a-b**). For each layer of such facemask, fibers, with a polydispersity corresponding to measured values, are randomly placed inside the simulation domain, where neighboring fibers are allowed to touch each other. In this way, the simulation domain becomes more realistic than the fiber geometry considered by, for example, Kuwabara. Simulations were repeated for different randomized domains, which allows statistical analysis of the simulation results. The capturing efficiency of an N95-facemask is studied by varying the droplet diameter from 10 nm to 1.0 μm for air inlet velocities varying from 0.1 m s^{-1} to 10 m s^{-1}. The simulated capturing efficiencies are compared to predictions made by the analytical models reviewed above and to experimental results found in literature.

2. Methodology

The 2D filter geometry is generated using the software MATLAB R2018b® and SolidWorks 2019®. A MATLAB script based on an existing function [34] is used to generate random diameter fibers and position them inside a 2D domain with a fixed domain height of 1 mm. To reproduce the actual morphology of the different layers of an N95-grade facemask, the script generates a geometry according to the thickness L, packing density α, and fiber diameter distribution $\overline{d_f} \pm \sigma_{df}$ of each layer. The layer properties, taken from Bałazy *et al.*, are listed in Table 1. These data were chosen because of the care taken by the authors to obtain statistically relevant measurement data and the availability of filter details, furthermore the data are quite representative for other work reported in literature (see e.g. the collected data in Davies [35] and Cheng et al. [36]). In the script, the packing density is defined as the ratio of the surface area occupied by fibers and the total surface area of the simulation geometry, as observed in a 2D projection of parallel fibers, see the example geometry in Fig. 3. This data is exported to SolidWorks using a macro, and the produced drawing is saved and exported to COMSOL Multiphysics 5.4, serving as the simulation geometry.

The model implemented in COMSOL Multiphysics is time-dependent and two-dimensional. For all simulations, the Reynolds number is found to be lower than 20, meaning that the assumption of laminar flow through the medium is correct. Hence, the flow is modeled using the incompressible Navier-Stokes and continuity equations which are solved using a linear piecewise interpolation method. Furthermore, the air is assumed to be a continuous medium for all droplet sizes. Particle tracking is implemented to simulate the forces acting on the droplets and to track the droplet position. The electrostatics module is used to model the electric field generated by electret fibers and allows the simulation of the dielectrophoretic force acting on the droplets. An example geometry of layer 3 of an N95-facemask is depicted in Fig. 3. The gray circles and the white rectangular area represent the polypropylene fiber domain and air domain, respectively. The arrows with accessory numbers point at boundaries on which different boundary conditions are applied.

The normal inflow (of air) boundary condition is set on boundary 1, and the velocity is varied between 0.1 m s^{-1} and 10 m s^{-1}, thereby matching the air inflow velocity of different expiratory events, such as breathing, talking, and coughing.[37,38] At this boundary, a fixed amount of 2-dimensional droplets is introduced with a diameter ranging from 10 nm to 1 μm. This diameter range is chosen because it spans the typical size of the SARS-CoV-2 virus up to the large virus-laden airborne droplets [39–42]. On boundary 2, a symmetry boundary condition is applied, meaning that the air and droplets can only escape at boundary 3, where an outlet boundary condition is applied. This outlet boundary condition fixes the pressure and also freezes the droplets, allowing the Navier-Stokes equations to be solved and the capturing efficiency to be evaluated. At the edge of each fiber, such as boundary 4, the no-slip

Table 1
Properties of the three fibrous layers of a N95-grade facemask. Data are taken from Bałazy *et al.*[28] ("Respirator A", see their Table 1).

Layer number k	Thickness $L \pm \sigma_L$ (mm)	Packing density α	Fiber diameter $\overline{d_f} \pm \sigma_{df}$ (μm)
1 (External)	0.31 ± 0.05	0.165	39.49 ± 1.80
2 (Middle)	1.77 ± 0.12	0.069	7.84 ± 2.00
3 (Internal)	1.05 ± 0.16	0.200	40.88 ± 2.26

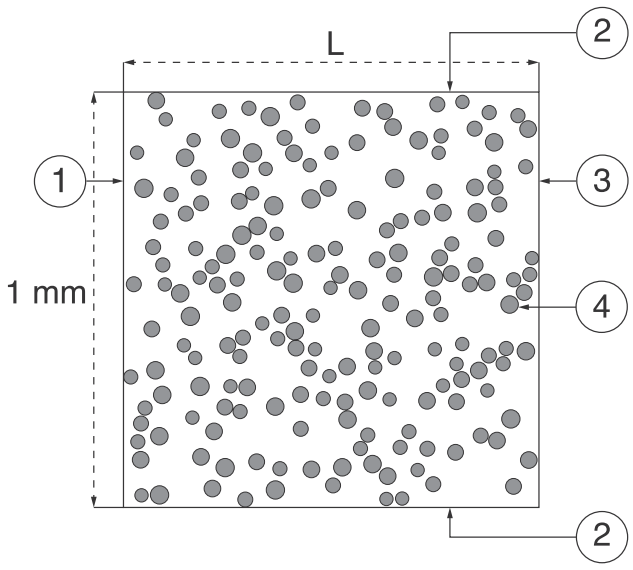

Fig. 3. An example of a simulation geometry of layer 3 of an N95-facemask. The gray circles depict the fibers' cross-section, and the white area depicts the air domain in between the fibers. The numbers with arrows point at boundaries where certain boundary conditions are applied. The height of the simulation geometry is set to 1 mm, whereas the thickness L is set according to the specifications of each fibrous layer. The packing density is defined as the total gray area divided by the area of the simulation geometry (see text).

condition guarantees no net air velocity. Droplets contacting the fiber edge become instantly static, thereby mimicking the capture of the droplet by a fiber.

Electret fibers are treated as a linear dielectric with a net permanent polarization that is directed upstream for all fibers in the geometry. Because in literature there is no consensus about the polarization density σ of electret fibers, this parameter is assumed to be of the order of $1 \cdot 10^{-4} Cm^{-2}$. The physical parameters of the fibers, air and droplets used in the model are listed in Table 2, in which the liquid parameters correspond to the properties of human saliva, and the temperature of the air is set to the average temperature of air exhaled by humans.

The geometry is discretized using a free triangular mesh and is refined at the air-fiber interface using the boundary layer node. A mesh convergence study has been performed to ensure that the mesh has a sufficient spatial resolution to solve the differential equations and simulate the droplet capturing process. A default stationary solver calculates the pressure distribution, velocity field, and electrostatic field in the air domain. These solutions are subsequently used in a default time-dependent study to uni-directionally solve the droplet trajectories by calculating the Stokes drag and the dielectrophoretic and Brownian forces acting on the droplets.

Table 2
Relevant physical parameters used in this work.

Droplet density[43,44]	$993 kgm^{-3}$
Droplet dynamic viscosity[45,46]	$1.69 \cdot 10^{-3} Pas$
Droplet surface tension[46]	$65.7 \cdot 10^{-3} Nm^{-1}$
Dielectric constant of the droplets[47]	75
Air temperature[43,48]	$34^{\circ} C$
Air dynamic viscosity[43]	$1.9 \cdot 10^{-5} Pas$
Air density[43]	$9.8 \cdot 10^{-1} kgm^{-3}$
Dielectric constant of air	1.0
Electrical conductivity of air	$8 \cdot 10^{-15} Sm^{-1}$
Polypropylene density	$912 kgm^{-3}$
Dielectric constant of Polypropylene[49]	2.3
Polarization density of Polypropylene	$1 \cdot 10^{-4} Cm^{-2}$

Using a randomized simulation geometry for each of the three layers on an N95-facemask, the filtering efficiency of each layer is analyzed separately. Every time a simulation is ran, a new random simulation domain is generated by the Matlab script, i.e. the fiber's size and position are randomized. To obtain statistically meaningful simulation results, this process is repeated n_s times and the results are averaged. The normal inflow velocity of air is fixed to determine the minimum number of simulations to assure statistically meaningful results. The minimum number of simulations is reached once the mean pressure drop across a filtering layer reaches a plateau.

The filtration efficiency of each layer k has been calculated for different inlet velocities and a range of droplet diameters, for each randomized filtering medium. The filtering efficiency E_k of layer k is calculated as $E_k = 1 - \frac{n_{out}}{n_{in}}$, with n_{in} the number of droplets at the inlet (boundary 1 in Fig. 3) and n_{out} the number of droplets reaching the outlet (boundary 3 in Fig. 3). Another parameter used to quantify the filtering performance is the particle penetration P_k, which is defined as $P_k = 1 - E_k = \frac{n_{out}}{n_{in}}$ [15,16].

The average $\overline{X}$ and standard deviation $\sigma_{X,k}$ (where X is E or P) for each layer k are calculated as $\overline{X_k} = \frac{1}{n_s}\sum_{i=1}^{n_s} X_i$ and $\sigma_{X,k} = \sqrt{\frac{\sum_{i=1}^{n_s}\left(\overline{X_k} - X_i\right)^2}{n_s - 1}}$, with X_i the value of X obtained from simulation i. The total particle penetration $\overline{P}$ of the N95-facemask is calculated as $\overline{P} = \prod_{k=1}^{3} P_k$, and the total capturing efficiency as $\overline{E} = 1 - \overline{P}$. The standard deviation of the total capturing efficiency $\overline{E}$ and $\overline{P}$ are calculated as $\sigma_E = \sigma_P = \overline{P}\sqrt{\left(\frac{\sigma_{P1}}{\overline{P_1}}\right)^2 + \left(\frac{\sigma_{P2}}{\overline{P_2}}\right)^2 + \left(\frac{\sigma_{P3}}{\overline{P_3}}\right)^2}$.

3. Results and discussion.

3.1. Filtering efficiency – No electret-based filter

The filtering efficiency of the different layers of an N95-grade facemask is analyzed first without considering the electrostatic interaction between the fibers and droplets. Using our model and analysis method, the mean and standard deviation of the capturing efficiency of each layer k are determined. These values are compared to the results that we obtained by the depth-filtration theory described in the introduction. Fig. 4 shows the capturing efficiencies E_k for all three layers as a function of the droplet diameter d_d for three different air inflow velocities V. The modeled capturing efficiency $\overline{E_k}$ shows the same trend as that predicted by the depth-filtration theory but fits only for the intermediate droplet sizes and low flow velocities. Presumably, discrepancies arise because the depth-filtration theory assumes homogeneously distributed and monodisperse fibers and considers each capturing mechanism to act independently on the droplets, whereas our numerical model takes randomness into account in a statistical manner. Unfortunately there are no experimental data available of individual layers to verify the data in this figure.

Compared to layers 1 and 3, the capturing efficiency of layer 2 is higher for the considered range of droplet diameters and flow velocities. This is due to the fact that the overall capturing efficiency of a layer scales exponentially with the factor $\frac{4\alpha L}{\pi \overline{d_f}(1-\alpha)}$ (see above). Assuming that the single fiber capturing efficiency in all three layers is equal, and taking the numbers given in Table 1, it follows that for layer 2 this factor is approximately 2.6 and 10.8 times larger than that for layers 3 and 1, respectively. On top of this, layer 2 contains the smallest fibers and therefore the curvature of the air streamlines in the vicinity of the fibers is larger than in the other layers, meaning that droplets of all sizes are captured more efficiently by means of interception. This effect is also predicted by Lee and Liu, and others, who derived that this capturing mechanism scales with the droplet to fiber diameter ratio.[20,25]

For the smallest droplets, which have a low inertia, capturing by

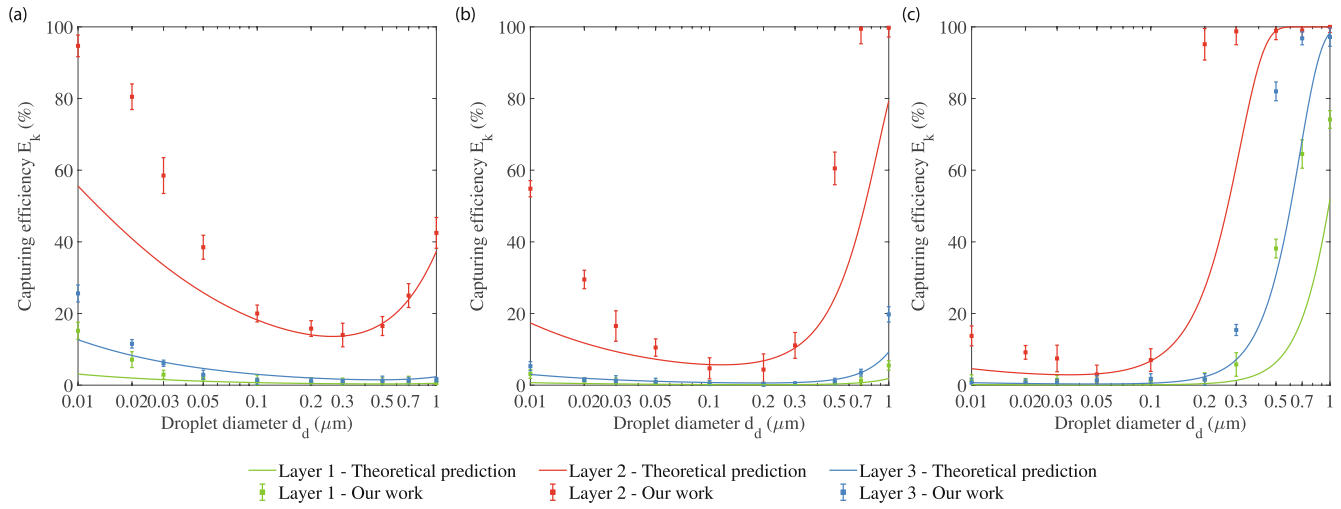

Fig. 4. Capturing efficiency E_k for a normal inflow velocity of (a) 0.1 m s^{-1}, (b) 1.0 m s^{-1} and (c) 10 m s^{-1}, as a function of the droplet diameter d_d. The solid lines represent the capturing efficiency calculated according to the depth-filtration theory explained in the introduction. The error bars show the standard deviation of the determined capturing efficiency E_k at each point in the graph, which are derived from the repeated randomization process described in Methodology.

inertial impaction and interception is less likely. Although it is assumed that the predominant capturing mechanism for small droplets occurs by means of diffusion, the work from Lee and Liu, [20] and others[24,25] suggests that diffusion-enhanced interception is likely to happen as well. At higher airflow rates, droplets are advected by the airflow rather than that they traverse a diffusive path.[15,16] This phenomenon is observed in Fig. 4, in which the capturing efficiency of small droplets for all three different layers decreases for increasing flow rate. This effect can also be understood as follows: for large Péclet numbers, the single fiber capturing efficiency by means of diffusion scales approximately as $V^{-2/3}$. The fiber diameter in layer 2 is approximately a factor of 5 smaller than that in layers 1 and 3 (Table 1). Therefore, the Péclet number for layer 2 is a factor of 5 larger. Even though the packing density of layer 2 is the lowest, the single fiber capturing efficiency by means of diffusion is the highest for fibers in layer 2 (Fig. 4). Because the fiber diameter in layers 1 and 3 are approximately equal, the Péclet numbers in these layers are approximately equal too. As a result, the single fiber capturing efficiency through diffusion and interception is approximately equal in layers 1 and 3. Layer 3 has a somewhat higher filtering efficiency, mainly because its layer thickness is approximately 3 times that of layer 1.

For larger droplet sizes and all air inflow velocities V, the capturing efficiency in all three layers increases. Furthermore, at higher flow velocities, the efficiency rise occurs at smaller droplet sizes. This phenomenon is due to the increase of the capturing efficiency by means of inertial impaction. Because the fibers in layer 2 are approximately 5 times smaller in diameter compared to the fibers in layers 1 and 3, the Stokes number of the droplets moving in layer 2 is approximately 5 times larger than in the other two layers. Therefore, the single fiber

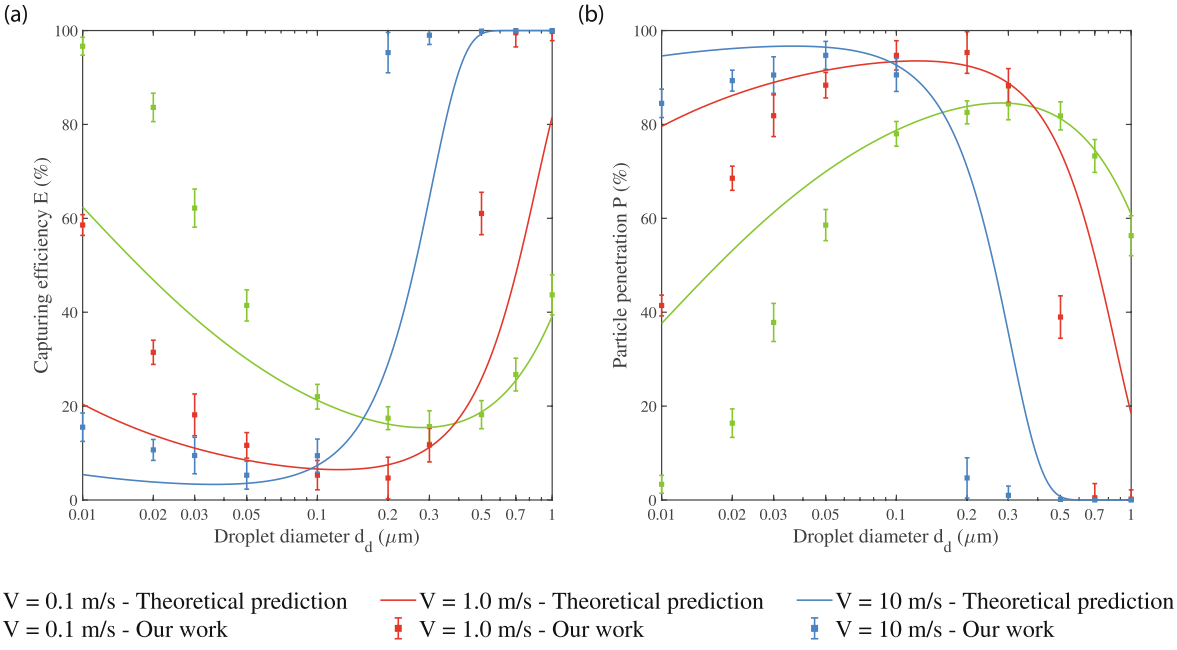

Fig. 5. The total capturing efficiency E (a) and particle penetration P (b) for the three mask layers in series, plotted as a function of the droplet diameter d_d and for different normal inflow velocities. The error bars for our simulation results denote the standard deviation calculated from the simulations for different randomized fiber configurations, as described in Methodology. The solid lines depict the calculated data obtained using the depth-filtration theory. The solid lines are data obtained by the depth-filtration theory.

capturing efficiency by means of inertial impaction is higher in layer 2. This effect is explained in the work of Zhu et al., where the single fiber capturing efficiency by means of inertial impaction scales quadratically and linearly with the Stokes number.[18] Although the packing density in layer 2 is approximately 3 times lower than that in the other two layers, the much higher Stokes number assures that inertial impaction is more effective in layer 2.

In Fig. 5, the total capturing efficiency E and particle penetration P of the N95-grade facemask is plotted as a function of droplet diameter d_d for different flow velocities V. The minimum in the capturing efficiency observed for each layer E_k (Fig. 4) and therewith the minimum of the total capturing efficiency E (Fig. 5**a**) decreases with increasing flow velocity. Furthermore, the minimum is found for intermediate droplet sizes, and shifts to smaller droplet sizes for increasing flow velocity. As discussed above, this shift is understood because the single fiber capturing efficiency by means of inertial impaction increases,[18] whereas the single fiber capturing efficiency by means of diffusion decreases at higher flow velocities.[20] These effects therefore dominate the most penetrating particle size (MPPS). At a flow velocity $V = 0.1\text{ms}^{-1}$, the particle penetration P of droplets with radius $d_d = 0.3\mu$m is above 80% (Fig. 5**b**), demonstrating the important finding that mask filters relying only on mechanical filtering do not conform to the N95 standard set by the NIOSH.[12,28]

3.2. Filtering efficiency – Electret-based filter (N95-grade facemask)

The simulations are repeated, this time treating the fibers in the second layer as electrets. The droplets are assumed to be uncharged, therefore only mechanical capturing and capturing by means of dielectrophoresis is considered. Fig. 6**b** shows the electret-including capturing efficiency E_2 as a function of the droplet diameter d_d and air inflow velocity V. For comparison, the capturing efficiency without electrostatic interaction is re-plotted in Fig. 6**a**. The increase of the filtering efficiency due to the electrostatic capturing mechanism is evident, as the filtration efficiency for all droplet diameters and airflow velocities is increased. In particular, droplets with sizes that are not filtered effectively by means of diffusion and interception are filtered rather efficiently due to the electrostatic interaction. At low air inflow velocities, the advected droplets have lower kinetic energy, and thus the droplets are easier deflected by the dielectrophoretic force. Therefore, filtering by electret fibers (Fig. 6**b**) is more efficient for low air velocities. These effects are also predicted by Lathrache and Fissan, [29–31]. who derived that the capturing efficiency by means of electrostatic interaction scales nonlinearly with the droplet diameter d_d and air inflow velocity V.

The deviation between the results of depth-filtration theory (including the electret effect calculated as explained in the introduction) and our simulated capturing efficiency E_2 becomes larger once the fibers are treated as electrets. In a fiber bed with randomly positioned electret fibers, the electric field generated by a single electret fiber is altered in a non-linear manner by neighboring electret fibers. This effect changes the single electrostatic fiber capturing efficiency. However, such an effect cannot be included in a straightforward way in depth-filtration theory and therefore it is concluded that the mentioned increased deviation is mainly due to inadequate theoretical description of the single fiber capturing efficiency utilizing dielectrophoresis. More complex models are needed, which until now are scarce in literature. Only recently, the first attempt in this direction has been published [50].

The total capturing efficiency E and particle penetration P of an N95-grade facemask are computed, with the results shown in Fig. 7**a** and Fig. 7**b**, respectively. It is evident that the electrostatic interaction is essential for a high droplet capturing efficiency. For example, the minimum capturing efficiency of the simulated N95-facemask filter is 93% at an air inflow velocity of $V = 0.1ms^{-1}$, whereas this minimum without the electrostatic interaction reaches only 15% (Fig. 5**a**). At this air velocity, the MPPS shifts from approximately $d_d = 0.3\mu$m to$d_d = 0.05\mu$m, also indicating the importance of the electret fiber web [10] to filter smaller aerosols and therewith reduce the spreading rate of respiratory viruses like SARS-CoV-2.

3.3. Filtering efficiency N95-grade facemask – Model vs. experiments.

Lastly, we compared the particle penetration predicted by our model with the experimental data reproduced from Bałazy et al. [28] These

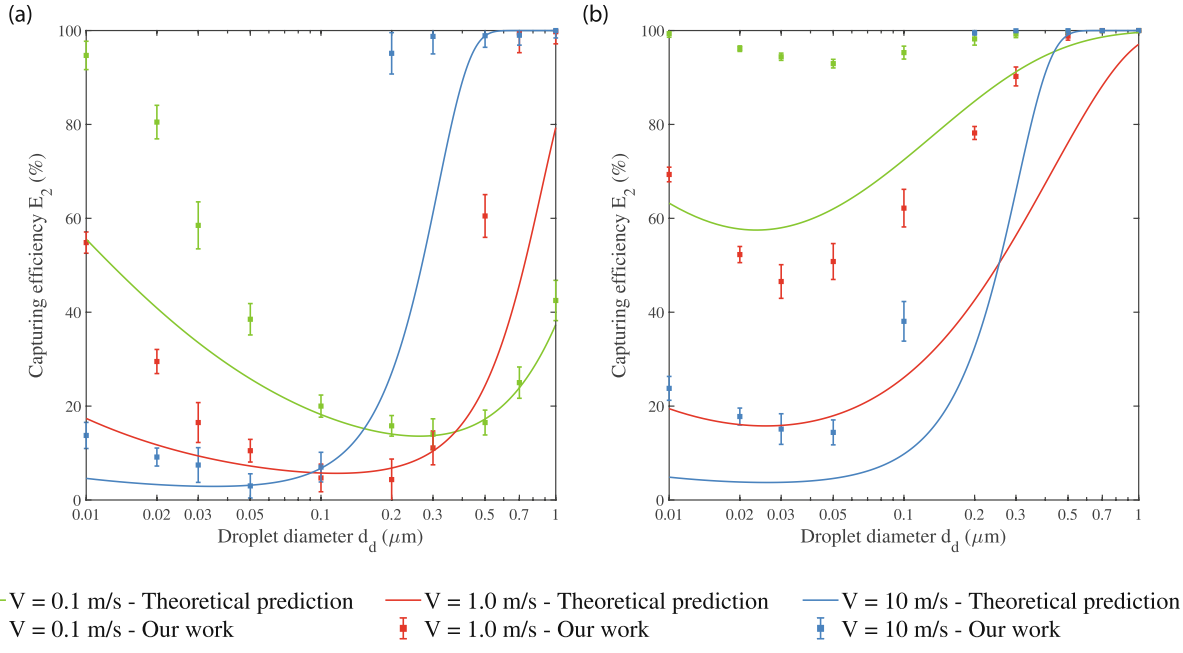

Fig. 6. The capturing efficiency E_2 plotted as a function of the droplet diameter d_d for various airflow velocities for layer 2. In (a), the fiber web consists of non-electret fibers (i.e., this figure compiles the red lines and points of the graphs in Fig. 4), whereas in (b), the fibers are considered as electrets. The error bars represent the calculated standard deviation from our series of randomized simulations (see Methodology). (For interpretation of the references to color in this figure legend, the reader is referred to the web version of this article.)

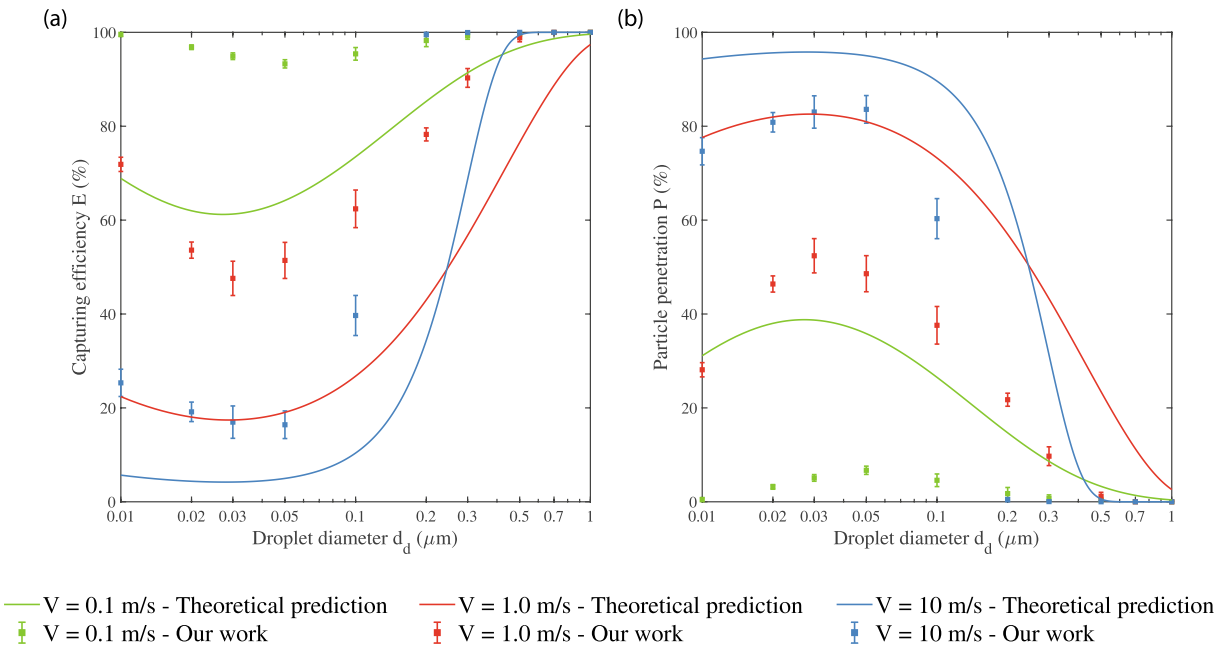

Fig. 7. In (a) the simulated and theoretically predicted capturing efficiency E and in (b) particle penetration P of an N95-grade facemask, plotted as a function of the droplet diameter d_d for different air inflow velocities.V.

authors measured the penetration of uncharged NaCl particles with diameters d_d ranging from 10 nm to 0.6 μm, under a volumetric air inflow rate of 85 L min^{-1}, which corresponds to a normal average air inflow velocity $V \approx 0.13 ms^{-1}$ [28]. The experiments proved that an N95-grade facemask could exceed the 5% particle penetration threshold, even when the facemask seals perfectly to the wearers' face. Above we have already explained the reasons to choose these data, which we consider representative for the state of the art of N95-grade masks. In Fig. 8, Bałazy et al.'s experimentally obtained particle penetration data is reproduced and plotted together with our simulation results. The slight difference between the normal air inflow velocities in our simulations (0.1 m s^{-1}) and experiments (0.13 m s^{-1}) is considered negligible. It can be observed that our model with the statistical analysis method predicts the overall particle penetration quite accurately, with a slight overestimation around the maximum particle penetration. Because the MPPS reduces from $d_d = 0.3\mu m$ to $d_d = 0.05\mu m$ due to droplet caputuring by means of dielectrophoresis, it is expected that our model underrated this effect. The model from Lathrache and Fissan used to calculate the single fiber capturing efficiency by means of dielectrophoresis scales with the square of the line charge density [29–31]. Hence, it is expected that our model scales with the square of the product of the fiber diameter and polarization density. These observations makes us confident that the estimated polarization density $P = 1 \cdot 10^{-4} Cm^{-2}$ is in the right range, and that the fiber diameter is correctly randomized.

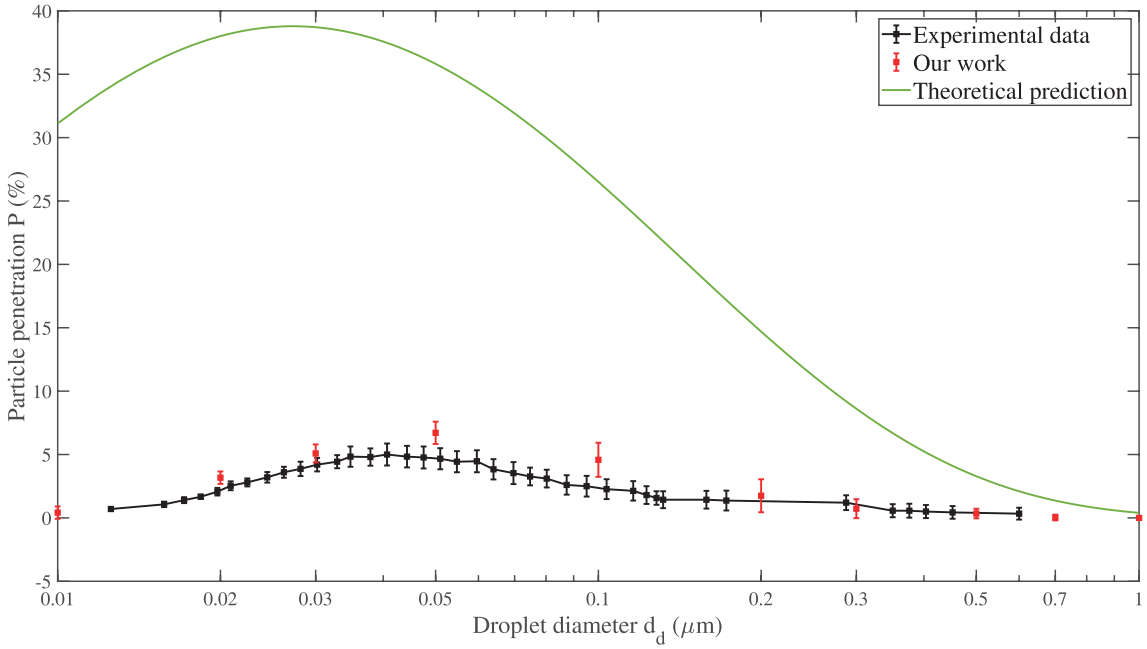

Fig. 8. Numerically predicted particle penetration (for an air inflow velocity of $V = 0.1 ms^{-1}$) plotted together with the experimentally obtained particle penetration (at an air inflow velocity of $V = 0.13 ms^{-1}$) reproduced from Bałazy et al. ("Respirator A").[28]

The model predicts that the particle penetration in N95-grade facemasks exceeds the 5% threshold for droplets with a diameter smaller than 300 nm. Note that this is not covered by the N95 grade, which specifies the 5% threshold at 300 nm. It is not yet clear how significant these small droplets contribute to the transmission of respiratory viruses. It has been argued by Mao *et al.* that, although the viral concentrations in small droplets are not precisely known, it seems likely that smaller droplets have a relatively small viral load [51]. Thus, even if there might be a larger amount of smaller droplets, their total volume is smaller than that of larger droplets, which might render them less infectious. On the other hand, the same authors also mention that smaller droplets penetrate deeper into the lungs, which would imply a higher probability of infecting an individual. Furthermore, our results in e.g. Fig. 7**b** show that even with the electret functionality, the N95 facemask is ineffective in capturing the smaller particles at air velocities of 1.0 m s^{-1}, which are the conditions during speaking, i.e. normal human interaction. This indicates that the relevance of the droplets in the smallest size range should perhaps not be underestimated.

To conclude, we think that a model as presented by us is accurate and reliable enough to predict, with limited computing effort, the different contributions to the filtering efficiency of facemasks for aerosol droplets with different diameters and different air velocities. In this way, it will be very helpful in the design of improved multilayer filters with a specific particle capturing window.

4. Conclusions

In this work, existing analytical models to predict the single fiber capturing efficiency due to different capturing mechanisms were reviewed. The essential capturing mechanisms, being interception, inertial impaction, Brownian diffusion, and dielectrophoresis, were included in a 2D computational model to simulate the capturing efficiency of the individual layers as well as the total capturing efficiency of a 3-layer N95-grade facemask. The model represents the fibrous layers as parallel cylindrical fibers with randomly distributed fiber diameter and position, and design parameters such as packing density, layer thickness, and fiber diameter and its distribution reported in the literature were used to reproduce a real N95-grade filter morphology and dimensions. The essential contribution of the electret functionality of the center mask layer clearly stands out, especially for filtering in the smaller range of droplets. The simulation results were compared with the predictions of depth filtration theory, commonly used in literature. Good correspondence is found between the simulated capturing efficiency and experimental particle capturing data from literature.

Our simulations also reveal that an N95-grade facemask does not adequately filter nanometric droplets. If droplets smaller than 300 nm turn out to be important to combat the spread of airborne diseases such as COVID-19, new facemask designs will be required. Designs with increasing filtering efficiency have been reported, such as filters consisting of nanofibers rather than microfibers.[11,52,53,54] Although a nanofiber web can assure a high filtering efficiency, it significantly increases the air resistance, which reduces the wearing comfort of such a mask. Furthermore, such nanofiber web clogs sooner, thereby also rapidly increasing the air resistance. Multilayer filters, analogous to N95-grade facemasks with an interlayer spacing, are proposed to reduce the pressure drop across the filters [52]. It is envisioned that the minimum capturing efficiency could be increased, and the MPPS could be reduced by adding another electret fiber layer, changing the morphology or layer thickness of the electret fiber web of an N95-grade facemask. Electret fibers with a larger polarization density increase the electric field strength and enhance the electrostatic capturing efficiency [55]. The presented model and analysis method will help studies towards a more effective aerosol filter for a desired diameter range and air inflow velocity.

CRediT authorship contribution statement

B.T.H. Borgelink: Conceptualization, Methodology, Validation, Visualization. **A.E. Carchia:** Conceptualization, Methodology, Validation, Visualization. **J.F. Hernández-Sánchez:** Conceptualization, Methodology. **D. Caputo:** Conceptualization, Methodology. **J.G.E. Gardeniers:** Conceptualization, Methodology. **A. Susarrey-Arce:** Conceptualization, Methodology.

Declaration of Competing Interest

The authors declare that they have no known competing financial interests or personal relationships that could have appeared to influence the work reported in this paper.

Acknowledgment

B.T.H.B., A.S.-A., and J.G.E.G. received funding from the European Research Council (ERC) under the European Union's Horizon 2020 research and innovation program (grant agreement no. 742004). The authors thank Francesca Lucilla Ciano (freelance graphic web designer) for the artwork.

References

[1] WHO Coronavirus (COVID-19) Dashboard | WHO Coronavirus (COVID-19) Dashboard With Vaccination Data, (n.d.). https://covid19.who.int/ (accessed July 29, 2021).
[2] L. Luo, D. Liu, X. Liao, X. Wu, Q. Jing, J. Zheng, F. Liu, S. Yang, B. Bi, Z. Li, J. Liu, W. Song, W. Zhu, Z. Wang, X. Zhang, P. Chen, H. Liu, X. Cheng, M. Cai, Q. Huang, P. Yang, X. Yang, Z. Han, J. Tang, Y. Ma, C. Mao, Modes of contact and risk of transmission in COVID-19 among close contacts, MedRxiv. (2020), https://doi.org/10.1101/2020.03.24.20042606.
[3] K.P. Fennelly, Particle sizes of infectious aerosols: implications for infection control, Lancet Respir. Med. 8 (9) (2020) 914–924, https://doi.org/10.1016/S2213-2600(20)30323-4.
[4] L. Morawska, D.K. Milton, It Is Time to Address Airborne Transmission of Coronavirus Disease 2019 (COVID-19), Clin. Infect. Dis. 71 (2020) 2311–2313. https://doi.org/10.1093/cid/ciaa939.
[5] R.V. Tso, B.J. Cowling, Importance of Face Masks for COVID-19: A Call for Effective Public Education, Clin. Infect. Dis. 71 (2020) 2195–2198, https://doi.org/10.1093/cid/ciaa593.
[6] S. Rab, M. Javaid, A. Haleem, R. Vaishya, Face masks are new normal after COVID-19 pandemic, Diabetes Metab. Syndr. Clin, Res. Rev. 14 (6) (2020) 1617–1619, https://doi.org/10.1016/j.dsx.2020.08.021.
[7] E. Bontempi, The europe second wave of COVID-19 infection and the Italy "strange" situation, Environ. Res. 193 (2021) 110476, https://doi.org/10.1016/j.envres.2020.110476.
[8] L. Peeples, Face masks: what the data say, Nature. 586 (7828) (2020) 186–189, https://doi.org/10.1038/d41586-020-02801-8.
[9] C.N. Ngonghala, E. Iboi, S. Eikenberry, M. Scotch, C.R. MacIntyre, M.H. Bonds, A. B. Gumel, Mathematical assessment of the impact of non-pharmaceutical interventions on curtailing the 2019 novel Coronavirus, Math. Biosci. 325 (2020) 108364, https://doi.org/10.1016/j.mbs.2020.108364.
[10] A. Bałazy, M. Toivola, A. Adhikari, S.K. Sivasubramani, T. Reponen, S. A. Grinshpun, Do N95 respirators provide 95% protection level against airborne viruses, and how adequate are surgical masks? Am. J. Infect. Control. 34 (2) (2006) 51–57, https://doi.org/10.1016/j.ajic.2005.08.018.
[11] W.-F. Leung, Q. Sun, Charged PVDF multilayer nanofiber filter in filtering simulated airborne novel coronavirus (COVID-19) using ambient nano-aerosols, Sep. Purif. Technol. 245 (2020) 116887, https://doi.org/10.1016/j.seppur.2020.116887.
[12] 42 CFR Appendix B to Part 84 - Application-Based Respirator Certification Fees - Content Details - CFR-2019-title42-vol1-part84-appB, (n.d.). https://www.govinfo.gov/app/details/CFR-2019-title42-vol1/CFR-2019-title42-vol1-part84-appB/summary (accessed February 5, 2021).
[13] A. Rengasamy, Z. Zhuang, R. BerryAnn, Respiratory protection against bioaerosols: Literature review and research needs, Am. J. Infect. Control. 32 (6) (2004) 345–354, https://doi.org/10.1016/j.ajic.2004.04.199.
[14] C.-S. Wang, Electrostatic forces in fibrous filters - A review, Powder Technol. 118 (1-2) (2001) 166–170, https://doi.org/10.1016/S0032-5910(01)00307-2.
[15] I.M. Hutten, Filtration Mechanisms and Theory, in: Handb. Nonwoven Filter Media, Elsevier, 2007: pp. 29–70. https://doi.org/10.1016/b978-185617441-1/50017-2.
[16] T.J. Ptak, in: Fibrous Filter Media, Elsevier, 2017, pp. 3–26, https://doi.org/10.1016/B978-0-08-100573-6.00002-2.

[17] S. Kuwabara, The Forces experienced by Randomly Distributed Parallel Circular Cylinders or Spheres in a Viscous Flow at Small Reynolds Numbers, J. Phys. Soc. Japan. 14 (4) (1959) 527–532, https://doi.org/10.1143/JPSJ.14.527.
[18] C. Zhu, C.H. Lin, C.S. Cheung, Inertial impaction-dominated fibrous filtration with rectangular or cylindrical fibers, in: Powder Technol., Elsevier Sequoia SA, 2000: pp. 149–162. https://doi.org/10.1016/S0032-5910(99)00315-0.
[19] M.D. Allen, O.G. Raabe, Re-evaluation of millikan's oil drop data for the motion of small particles in air, J. Aerosol Sci. 13 (6) (1982) 537–547, https://doi.org/10.1016/0021-8502(82)90019-2.
[20] K.W. Lee, B.Y.H. Liu, Theoretical study of aerosol filtration by fibrous filters, Aerosol Sci. Technol. 1 (2) (1982) 147–161, https://doi.org/10.1080/02786828208958584.
[21] J.S. Andrade, U.M.S. Costa, M.P. Almeida, H.A. Makse, H.E. Stanley, Inertial effects on fluid flow through disordered porous media, Phys. Rev. Lett. 82 (26) (1999) 5249–5252, https://doi.org/10.1103/PhysRevLett.82.5249.
[22] C.-H. Hung, W.-F. Leung, Filtration of nano-aerosol using nanofiber filter under low Peclet number and transitional flow regime, Sep. Purif. Technol. 79 (1) (2011) 34–42, https://doi.org/10.1016/j.seppur.2011.03.008.
[23] R. GOUGEON, D. BOULAUD, A. RENOUX, Comparison of data from model fiber filters with diffusion, interception and inertial deposition models, Chem. Eng. Commun. 151 (1) (1996) 19–39, https://doi.org/10.1080/00986449608936539.
[24] S. Payet, D. Boulaud, G. Madelaine, A. Renoux, Penetration and pressure drop of a HEPA filter during loading with submicron liquid particles, J. Aerosol Sci. 23 (7) (1992) 723–735, https://doi.org/10.1016/0021-8502(92)90039-X.
[25] B.Y.H. Liu, K.L. Rubow, Efficiency, pressure drop and figure of merit of high efficiency fibrous and membrane filter media, in: Vth World Filtr. Congr., 1990: pp. 112–119. http://membranes.edu.au/vital/access/manager/Repository/memre:360 (accessed February 6, 2021).
[26] R.C. Brown, Capture of dust particles in filters by linedipole charged fibres, J. Aerosol Sci. 12 (4) (1981) 349–356, https://doi.org/10.1016/0021-8502(81)90024-0.
[27] R.C. Brown, Air Filtration -, 1st Edition, Elsevier Science, 1993.
[28] A. Bałazy, M. Toivola, T. Reponen, A. Podgórski, A. Zimmer, S.A. Grinshpun, Manikin-Based Performance Evaluation of N95 Filtering-Facepiece Respirators Challenged with Nanoparticles, Ann. Occup. Hyg. 50 (2005) 259–269, https://doi.org/10.1093/annhyg/mei058.
[29] R. Lathrache, H.J. Fissan, S. Neumann, Deposition of submicron particles on electrically charged fibers, J. Aerosol Sci. 17 (3) (1986) 446–449, https://doi.org/10.1016/0021-8502(86)90127-8.
[30] R. Lathrache, H. Fissan, Fractional Penetrations for Electrostatically Charged Fibrous Filters in the Submicron Particle Size Range, Part. Part. Syst. Charact. 3 (2) (1986) 74–80, https://doi.org/10.1002/ppsc.v3:210.1002/ppsc.19860030206.
[31] R. Lathrache, H. Fissan, Enhancement of particle deposition in filters due to electrostatic effects, Filtr. Sep. 24 (1987) 418–422.
[32] C.N. Davies, Air filtration, Academic Press, London, 1973.
[33] K. Singha, S. Maity, M. Singha, S. pal, Computer Simulations of Textile Non-Woven Structures, Front. Sci. 2 (2012) 11–17, https://doi.org/10.5923/j.fs.20120202.03.
[34] Draw randomly centered circles of various sizes - File Exchange - MATLAB Central, (n.d.). https://it.mathworks.com/matlabcentral/fileexchange/70348-draw-randomly-centered-circles-of-various-sizes (accessed February 11, 2021).
[35] C.N. Davies, Filtration of aerosols, J. Aerosol Sci. 14 (2) (1983) 147–161, https://doi.org/10.1016/0021-8502(83)90039-3.
[36] Y. Cheng, N. Ma, C. Witt, S. Rapp, P.S. Wild, M.O. Andreae, U. Pöschl, H. Su, Face masks effectively limit the probability of SARS-CoV-2 transmission, Science (80-.). 372 (2021) 1439–1443. https://doi.org/10.1126/SCIENCE.ABG6296.
[37] S.-B. Kwon, J. Park, J. Jang, Y. Cho, D.-S. Park, C. Kim, G.-N. Bae, A. Jang, Study on the initial velocity distribution of exhaled air from coughing and speaking, Chemosphere. 87 (11) (2012) 1260–1264, https://doi.org/10.1016/j.chemosphere.2012.01.032.
[38] J.W. Tang, A.D. Nicolle, C.A. Klettner, J. Pantelic, L. Wang, A.B. Suhaimi, A.Y. L. Tan, G.W.X. Ong, R. Su, C. Sekhar, D.D.W. Cheong, K.W. Tham, E. Subbiah, Airflow Dynamics of Human Jets: Sneezing and Breathing - Potential Sources of Infectious Aerosols, PLoS One. 8 (4) (2013) e59970, https://doi.org/10.1371/journal.pone.005997010.1371/journal.pone.0059970.g00110.1371/journal.pone.0059970.g00210.1371/journal.pone.0059970.g00310.1371/journal.pone.0059970.g00410.1371/journal.pone.0059970.g00510.1371/journal.pone.0059970.g006.
[39] S. Anand, Y.S. Mayya, Size distribution of virus laden droplets from expiratory ejecta of infected subjects, Sci. Rep. 10 (2020) 1–9, https://doi.org/10.1038/s41598-020-78110-x.
[40] Y. Liu, Z. Ning, Y. Chen, M. Guo, Y. Liu, N.K. Gali, L. Sun, Y. Duan, J. Cai, D. Westerdahl, X. Liu, K. Xu, K.-fai. Ho, H. Kan, Q. Fu, K. Lan, Aerodynamic analysis of SARS-CoV-2 in two Wuhan hospitals, Nature. 582 (7813) (2020) 557–560, https://doi.org/10.1038/s41586-020-2271-3.
[41] G. Buonanno, L. Stabile, L. Morawska, Estimation of airborne viral emission: Quanta emission rate of SARS-CoV-2 for infection risk assessment, Environ. Int. 141 (2020) 105794, https://doi.org/10.1016/j.envint.2020.105794.
[42] J. Gralton, E. Tovey, M.-L. McLaws, W.D. Rawlinson, The role of particle size in aerosolised pathogen transmission: A review, J. Infect. 62 (1) (2011) 1–13, https://doi.org/10.1016/j.jinf.2010.11.010.
[43] L. Bourouiba, E. Dehandschoewercker, J.W.M. Bush, Violent expiratory events: On coughing and sneezing, J. Fluid Mech. 745 (2014) 537–563, https://doi.org/10.1017/jfm.2014.88.
[44] M. Nicas, W.W. Nazaroff, A. Hubbard, Toward Understanding the Risk of Secondary Airborne Infection: Emission of Respirable Pathogens, J. Occup. Environ. Hyg. 2 (3) (2005) 143–154, https://doi.org/10.1080/15459620590918466.
[45] R.P. Kusy, D.L. Schafer, Rheology of stimulated whole saliva in a typical pre-orthodontic sample population, J. Mater. Sci. Mater. Med. 6 (7) (1995) 385–389, https://doi.org/10.1007/BF00120278.
[46] T. Zhang, Study on Surface Tension and Evaporation Rate of Human Saliva, Saline, and Water Droplets, Graduate Theses, Dissertations, and Problem Reports. 2271 (2011). https://researchrepository.wvu.edu/etd/2271.
[47] S. Mehrotra, A. Kumbharkhane, A. Chaudhari, Permittivity Study of Bloods, Saliva, Tissue Cells, and Their Applications in Medical Instrumentations in the Detection of Oral Cancer, in: Bin. Polar Liq., Elsevier, 2017: pp. 429–439. https://doi.org/10.1016/b978-0-12-813253-1.00010-0.
[48] P. Höppe, Temperatures of expired air under varying climatic conditions, Int. J. Biometeorol. 25 (2) (1981) 127–132, https://doi.org/10.1007/BF02184460.
[49] S. Ahmed Dabbak, H. Illias, B. Ang, N. Abdul Latiff, M. Makmud, Electrical Properties of Polyethylene/Polypropylene Compounds for High-Voltage Insulation, Energies. 11 (2018) 1448. https://doi.org/10.3390/en11061448.
[50] L. Hou, A. Zhou, X. He, W. Li, Y. Fu, J. Zhang, CFD Simulation of the Filtration Performance of Fibrous Filter Considering Fiber Electric Potential Field, Trans. Tianjin Univ. 25 (5) (2019) 437–450, https://doi.org/10.1007/s12209-019-00218-7.
[51] N. Mao, C.K. An, L.Y. Guo, M. Wang, L. Guo, S.R. Guo, E.S. Long, Transmission risk of infectious droplets in physical spreading process at different times: A review, Build. Environ. 185 (2020) 107307, https://doi.org/10.1016/j.buildenv.2020.107307.
[52] J.J. Huang, Y. Tian, R. Wang, M. Tian, Y. Liao, Fabrication of bead-on-string polyacrylonitrile nanofibrous air filters with superior filtration efficiency and ultralow pressure drop, Sep. Purif. Technol. 237 (2020) 116377, https://doi.org/10.1016/j.seppur.2019.116377.
[53] R. Al-Attabi, Y. Morsi, Jürg.A. Schütz, D. Cornu, M. Maghe, L.F. Dumée, Flexible and reusable carbon nano-fibre membranes for airborne contaminants capture, Sci. Total Environ. 754 (2021) 142231, https://doi.org/10.1016/j.scitotenv.2020.142231.
[54] W.W.F. Leung, Q. Sun, Electrostatic charged nanofiber filter for filtering airborne novel coronavirus (COVID-19) and nano-aerosols, Sep. Purif. Technol. 250 (2020) 116886, https://doi.org/10.1016/j.seppur.2020.116886.
[55] J. Van Turnhout, W.J. Hoeneveld, J.-W. Adamse, L.M. Van Rossen, Electret Filters for High-Efficiency and High-Flow Air Cleaning, IEEE Trans. Ind. Appl. IA-17 IA-17 (2) (1981) 240–248, https://doi.org/10.1109/TIA.1981.4503932.